rijksuniversiteit groningen

faculteit Wiskunde en Natuurwetenschappen

Search for the proximity effect in MgB_2 epitaxial films on Mg(0001)

Bachelor Thesis Applied Physics

November '08

Student:

Olger Zwier

Supervisor:

Prof. Dr. P. Rudolf

Second supervisor:

Dr. C. Cepek

Abstract

Magnesium diboride was discovered in 2001 to superconduct at temperatures below 39 K, a very high critical temperature for a phonon-assisted superconductor, which MgB_2 has been determined to be. This research tries to determine the relation between the thickness of a sample of MgB_2 and its superconductive properties, a relation due to the proximity effect.

To produce thin MgB_2 films, we have deposited boron, or magnesium and boron simultaneously, on the Mg(0001) single crystal surface by means of molecular beam epitaxy (MBE). The growth took place in an ultra high vacuum (UHV) environment with a base pressure of below 2×10^{-10} mbar. The Mg(0001) substrate was thoroughly cleaned and ordered beforehand by several cycles of sputtering and annealing. In our conditions, the temperature of the substrate during growth must be kept between 498 and 513 K, a temperature range which allows Mg to react with boron and which is sufficiently low not to allow a massive Mg sublimation, which may hinder the MgB_2 formation (Mg vapour pressure in UHV:~ 10^{-9} mbar at 530K). Due to the experimental set-up, we were not able to measure directly the substrate temperature during annealing. As a consequence, during growth, the substrate temperature was increased up to when we observed the appearance of Mg mass in the residual gas analyser.

Analysis of the surface lattice geometry was done by Low Energy Electron Diffraction (LEED), growth rate and sample composition were characterized by Auger Electron Spectroscopy (AES) the surface was analyzed by Scanning Tunneling Microscopy (STM) and scanning electron spectroscopy (STS), at room temperature as well as at 4.2 K. The results obtained by this method show that while the stoichiometry of our MgB_2 film is correct, our growth procedure is not optimized to reliably prepare large regions of MgB_2. Scanning Tunneling Spectroscopy (STS) was also performed to search for the superconductive gap. These measurements, when they were not rendered unusable by noise, did however not show an adequate superconductive gap.

Several improvements are suggested to grow MgB_2 more successfully. A better control over the temperature of the sample during deposition is required, since the temperature window for epitaxial growth is very narrow. For the measurements by STS it is found imperative that the noise in the signal is minimized before reliable results are possible.

Table of contents

Introduction

1.1 History of superconductors

Sometimes quantum mechanics, usually only observable on a microscopic level, give rise to bulk effects that we can observe on a macroscopic scale. Superconductivity, the ability of certain materials to carry an electric current with zero electrical resistance at very low temperature, is a very prominent example. Ever since its discovery by Kamerling-Onnes in 1911 in mercury at a temperature of around 4K, understanding of the effect has grown substantially, and many more elements and compounds have been found to superconduct below their respective critical temperature (T_c), as can be seen in figure 1. As a rule, there are now two classes of superconductors. The low temperature superconductors are the simpler class, and are explained by BCS theory, proposed in 1957 by Bardeen, Cooper and Schrieffer. The second class, the high temperature "cuprate" superconductors, of which the first to be discovered in 1986 by Bednorz and Müller [1] was the La-Ba-Cu-O system that superconducts at 35K. This type of superconductor is still not fully understood yet.

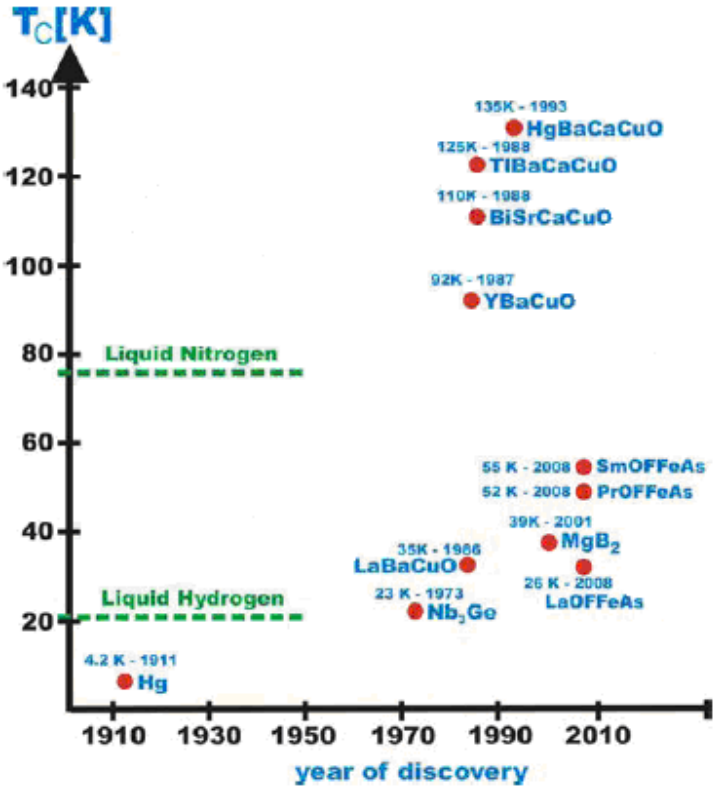

Figure 1: History of superconductors. Adapted from [3].

When in January 2001 the T_c in the simple metallic compound magnesium diboride (MgB_2) was found to be 39 K [2], interest in the material spread like wildfire in the scientific community. Taking notions from BCS theory, we know that the Tc in MgB_2 is about as high as we can expect it to be in a low temperature superconductor [4], which makes it a prime candidate for research concerning the nature of superconductivity, and practical applications, such as Josephson junctions.

1.2 Superconductivity in MgB_2 and motivation

As shown in figure 2b, the simple metallic compound MgB_2 has a structure very much like that of pure magnesium, shown in figure 2a, with planes filled with triangularly arranged magnesium atoms forming the basis of both materials. Where in magnesium these sheets are simply stacked to form a hexagonal structure as in figure 2a, in MgB_2 one in every two triangle-filled sheets of magnesium is replaced by a denser hexagonal sheet of boron atoms, as in figure 2b. The two materials of course have different lattice parameters, though they do not differ by much, especially in the in-plane direction. This seems to suggest that MgB_2 can be grown on top of clean magnesium in the (0001)-direction, with minimal stress and dilation of the MgB_2 near the interface. Indeed, in this research all MgB_2 was grown on Mg(0001).

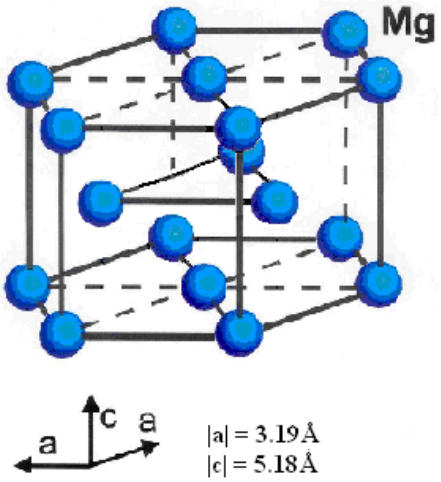

Figure 2a: Mg lattice structure (HCP).

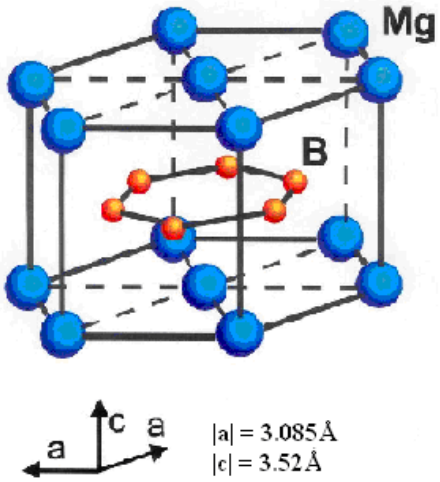

Figure 2b: MgB_2 lattice structure. Adapted from [5].

To do measurements on MgB_2, one needs samples with very few impurities, and a high degree of order for superconductivity to exist at all. Also, depending on the orientation of the grains of MgB_2, there are several distinct superconductive gaps one can see: both the indicated a- and c-directions have a distinct superconductive mechanism that can be seen simultaneously [6]. This makes a unidirectionally oriented sample a must, while only powder samples or randomly oriented samples are produced easily. In fact, up to now, there are no adequate techniques to produce such clean oriented bulk samples [7], and this motivates the choice of growing thin epitaxial films on a substrate.

The primary goal of this research is to find out how superconductivity in MgB_2 depends on the thickness of film, which means studying the role of the proximity effect [7]. This effect implies that Cooper pairs, the "particles" responsible for superconductivity, diffuse into the normal metal, and electronic excitations diffuse into the superconductor at the interface between superconductor and metal, the same way electrons and holes behave at an interface between two distinct metals. As a second motivation, research into the growing of adequate thin films by Molecular Beam Epitaxy (or "MBE") will prove helpful to future research, since this technique for producing MgB_2 is still young and has much room for improvement.

Experimental

2.1 The growth of MgB_2 thin films

Before growing thin films of MgB_2, the Mg(0001) substrate needs to be cleaned by several cycles of sputtering and annealing. During sputtering, the sample is bombarded by Argon ions that eject the top layers of the crystal. Since during this treatment disorder is introduced in the crystalline structure and argon is implanted in the sample, annealing the sample is necessary to restore surface order.
Then, for growing the films by means of molecular beam epitaxy on pure magnesium, there are two different For growing the films by means of molecular beam epitaxy on pure magnesium, there are two different approaches, both resulting in a sample with alternating sheets of boron and magnesium. As a simple method, one can steadily evaporate boron onto a magnesium substrate. The boron will diffuse into the magnesium and order itself into MgB_2, because of the reactivity of magnesium [4]. This technique can only be used to make a very thin film of up to two or three monolayers thick, before the magnesium is covered by boron and boron does not effectively diffuse any further. If thicker films are required, magnesium needs to be deposited along with the boron. Since magnesium has a very low sticking coefficient, the impinging flux needs to be strongly enriched in magnesium. Both techniques were used in this research.
For the deposition of magnesium and boron two types of evaporator are needed, aimed at the same spot on the substrate for co-deposition. Magnesium sublimes at sufficiently low temperatures in UHV (≈580K) that an atomic beam can be produced by resistively heating a crucible containing pure magnesium grains. The crucible presents a small aperture, which allows producing a beam. In our experiment we regulated the current through the filament of the crucible to have a magnesium deposition rate of 4 ML/h. The boron however would require very high currents that would melt parts of the evaporator for this method to work, so a different evaporator based on e-beam heating is used. A filament is wrapped around a rod of boron, electrons are accelerated from the filament to the rod, and focussed by the so-called Wehnelt onto the tip of the rod. Upon colliding the rod expels boron atoms from the top and onto the substrate. Our boron evaporator produces some two layers of boron every hour.

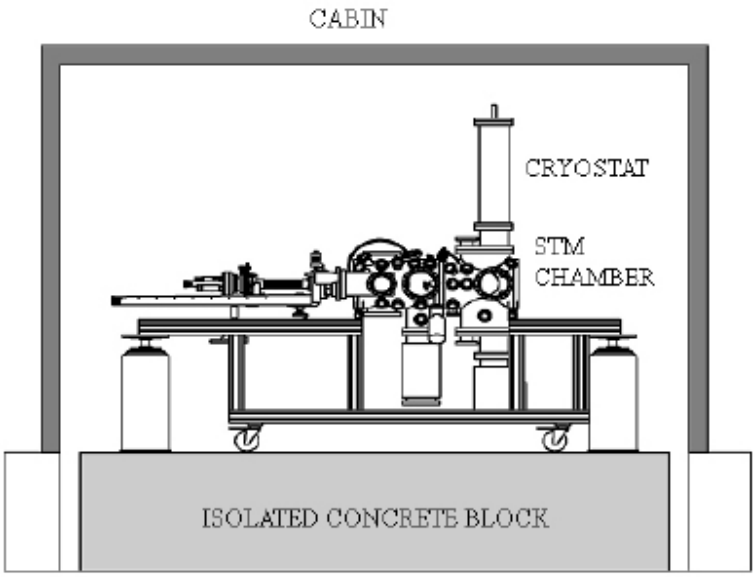

Figure 3: Schematical drawing of the UHV system used in the present thesis [8].

During both methods of deposition, the pressure needs to be kept below 10^{-9} mbar, to ensure that no residual gas atoms are incorporated in the film and the sample will be clean enough [7]. To this end, all growth and characterization is carried out in Ultra High Vacuum (UHV) conditions. In our research, the UHV system was composed of two large stainless steel chambers, the preparation chamber, used for preparing samples and characterizing them by Auger spectroscopy, and the main chamber, housing the low temperature STM. The two can be separated hermetically with a valve, so that one can simultaneously work on preparing a sample at room temperature, and perform STM or STS on another sample that has been cooled down. The pressure in the chambers is achieved by a turbo pump backed by a rotary pump, and ion pumps for both the chambers. The whole system is placed on an isolated floor and surrounded by a cabin to shield the STM from vibrations and electronic interference. The complete setup is shown in figure 3.
The other important parameter to control during growth besides pressure is the temperature of the substrate. The higher the temperature, the better ordered the film will be since the co-deposited atoms arrange themselves in their proper places. However, with the temperature a little over 513 K, the sticking coefficient of magnesium drops to 0. Additionally, if the sample temperature drops beneath 453 K magnesium and boron will not react properly and the sample will just be an ordinary conductor. The temperature is simply regulated by sending a current through the sample and thereby resistively heating it. The very small window of pressure versus temperature where MgB_2 can be grown, as seen in phase diagram shown figure 4, is the main reason why growing good samples is rather difficult. This is why before cooling down the sample to perform STM and STS measurements, we first assure ourselves that the sample is of the desired quality. Using Auger Electron Spectroscopy (AES), we can determine the stoichiometry of the film and if it is very thin, estimate its thickness. To check the crystalline quality of the sample, we use Low Energy Electron Diffraction (LEED). We also employed AES to determine the evaporation rates of our evaporators.

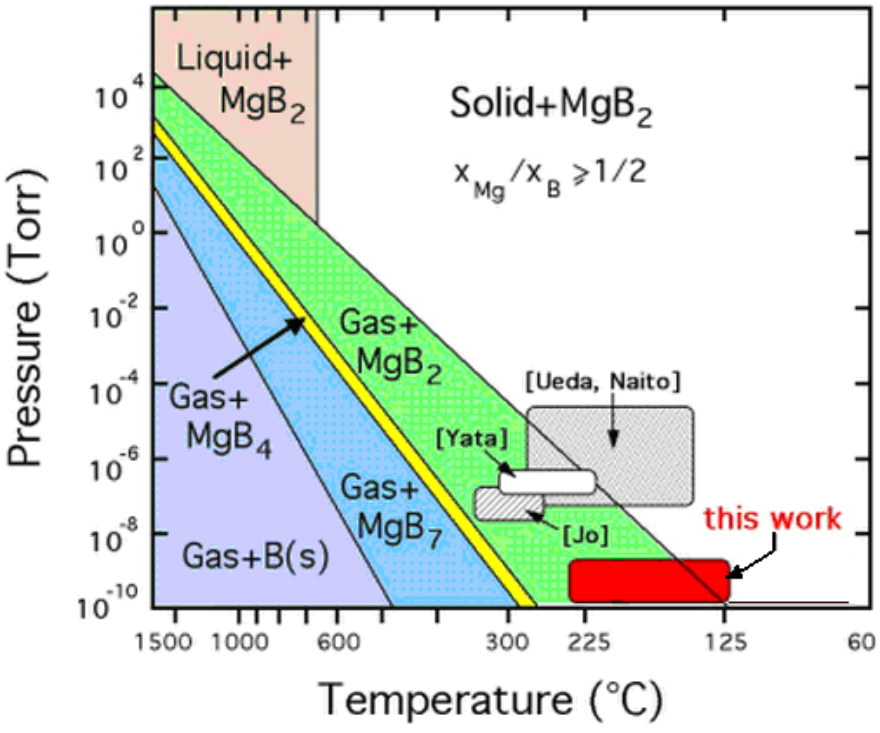

Figure 4: Phase diagram of Mg and B [9].

2.2 Analysis by AES

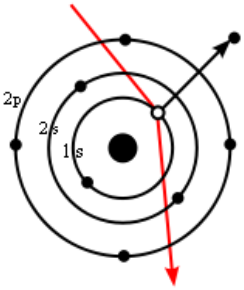

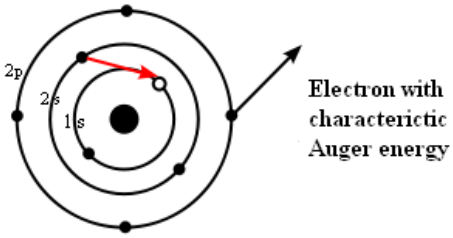

Figure 5a: Electron collision. **Figure 5b: Auger electron emission. Adapted from [10].**

As seen schematically in figure 5a, when a free electron of sufficient energy (red line) hits a core electron, both exit the electron cloud. This leaves the atom in an excited state with a core hole and an electron from an outer shell falls down to fill it. The energy freed in this process can be either emitted as a photon, or as shown in figure 5b, taken up by an outer shell electron which then escapes the atom. This final electron, called an Auger electron, has a very characteristic energy which depends on the initial energy of the core electron, which electron replaced it and which electron absorbed the energy.
To perform these measurements, electrons with a kinetic energy of 3 keV are fired at the sample by an electron gun. As shown in figure 6, the energy of the produced Auger electrons is analysed by first focussing them onto the entrance slit placed before the hemispheres by electronic lenses and slowing them down. Only electrons with a specific initial energy can pass through the hemispheres, which have a constant pass energy of 10 eV and are collected with a magnification device (here a channeltron) connected to a computer. Variation of the selected energy achieved through different decelleration voltages results in a graph of count rate N versus electron energy E. To see which elements are present at the sample surface, we look at the characteristic peaks for the Auger transitions in the graph of dN/dE versus electron energy. Also from the count rate versus energy plot one can determine the stoichiometry and growth speed.

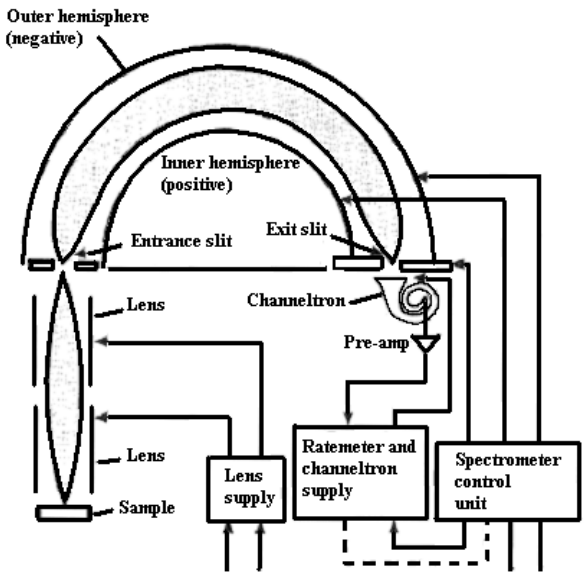

Figure 6: The electron analyser.

When Auger electrons pass through matter on their way to the surface, some of them will interact inelastically which results in an attenuation of the Auger peak intensities. This attenuation is obviously different when only one layer is traversed instead of two, which is again different from three, and so on. As sketched in figure 7, if our film grows layer by layer we can use this to determine the growth rate: if we record AES spectra as a function of deposition time, we will see a linear decrease of our substrate signal and a linear increase of our adsorbate signal. Once the first layer is completed, the attenuation of the substrate signal will be different and the signal of the first layer of the adsorbate will be attenuated by the growing second layer. Therefore we will see a kink in our plot of the AES intensity as a function of deposition time. Another kink will occur at the completion of the second layer, and from the times at which these kinks occur we can determine the growth rate and therefore calibrate our evaporators.
On the other hand, for thin films where the substrate signal is still visible, the AES spectra enable us to roughly estimate the thickness of the film if we know by how much the substrate signal intensity is attenuated. As an estimate of intensity we can take the count rate at the tip of the peak, with the background count rate subtracted. The Auger peak we chose to follow for the magnesium substrate corresponds to an $L_{2,3}M_1M_1$ transition (in X-ray notation), seen at 45 eV electron energy in a plot of dN/dE versus electron energy. This signal results from a hole in the 2p level, which is filled by an electron from the 3s level and the energy is given to the other electron in the 3s level [11]. For boron we used the peak corresponding to a $K_1L_{2,3}L_{2,3}$ transition, seen in a plot of dN/dE versus electron energy at 179 eV. This signal results from a hole in the 1s level, which is filled by an electron from the 2p level, which in turn gives its energy to another electron in the 2p level [11].

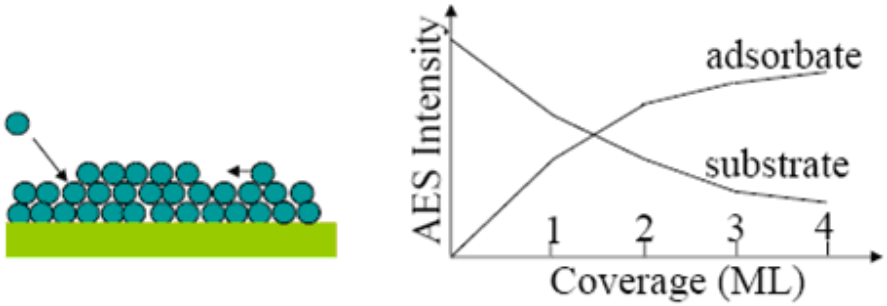

Figure 7: Schematic plot of the variation of intensity of substrate and adsorbate Auger peaks during layer-by-layer growth [12]

2.3 Analysis by LEED

To briefly explain how LEED works, one first needs an indication of how waves interfere when impinging on a lattice. When a sample is hit by waves, in the case of LEED electrons with a relatively low energy of around 100 eV, these diffract into all directions. In the simplest theoretical approximation, one can assume that they diffract only once, and because of the short mean free path of electrons with this energy, they do so on the topmost atoms of the sample. As figure 8a shows, in certain directions the waves will cancel each other since they are out of phase, and in others they will add because they are in phase, as in figure 8b. On the sample surface, this interference will take place in two dimensions along the two lattice vectors, with peaks of intensity distributed in both directions.

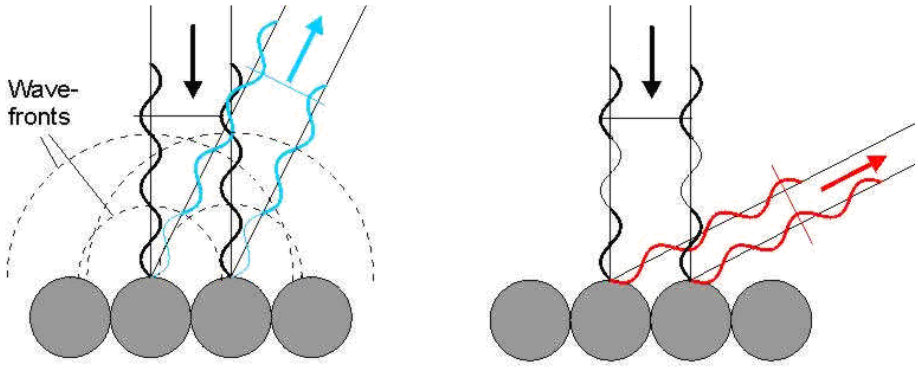

Figure 8a: Destructive interference. **Figure 8b: Constructive interference [13].**

To know the shape of this intensity peak pattern, directly related to the shape of the lattice when projected onto a fluorescent screen, it is convenient to introduce the so-called reciprocal lattice vectors, which form the basis for the reciprocal lattice. Not going into too much detail, suffice it to say that in two dimensions for each real or "direct" vector one can define a reciprocal lattice vector. Its length is inversely proportional to the original vector, and it is at a right angle to the other direct lattice vector. The resulting reciprocal lattice for the magnesium hexagonal structure is shown in figure 9, and can be seen to have the same shape as the direct lattice, except it has been flipped onto its side.

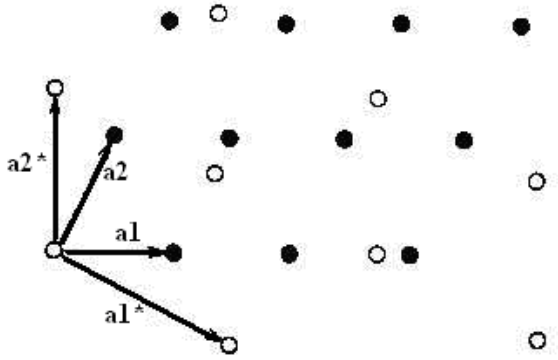

Figure 9: Direct lattice vectors (unstarred, black points) and reciprocal lattice vectors (starred, white spots) [13].

The pattern observed when performing LEED measurements on such a sample is exactly this reciprocal lattice. This is because along the directions of the reciprocal lattice vectors, the waves will add when their wave vectors differ by exactly one reciprocal lattice vector, a statement equivalent to saying the waves will add when in phase. Another way to put this is that the reciprocal lattice we see is a Fourier transform of the real lattice. Using this interpretation, we know that the size of the coherent domains is inversely proportional to the full width of the spots at half the maximum of the intensity of the spot [14]. The LEED spots are visible by eye from outside the vacuum system if the diffracted beams are intercepted by a fluorescent screen. After tuning of the electron energy and adjusting the sample position to have the electrons diffract from a well ordered region, spots appear on the screen where the electrons impact and form the pattern that characterises the sample lattice. A background of fluorescence, or visible noise, is also present, with an intensity that depends on the output of the electron gun, as well as the sample's crystalline order and temperature. The better the lattice, the sharper the pattern, the smaller the spots, and the weaker the noise. The resulting image is photographed with a simple hand-held camera.

3.1 Theory of superconductivity

In a classical conductor, electrons lose their energy through scattering off of impurities or phonons (lattice vibration quanta). In a superconductor however, there is no such scattering. To explain this, Leon Cooper proposed that there might exist a binding force, that could bind electrons together in the superconductor [15]. This binding force, its exact nature unknown at the time it was proposed, would turn pairs of fermionic electrons with half-integer spin values into bosons, with an integer spin value. These bosons, being free from fermionic exclusion principles, would be able to condensate into the ground state and so fall under the medium's Fermi level, where the small scattering excitations take place. When the temperature drops and thermal fluctuations, which have energy k_bT, become smaller than the energy holding the two electrons together, these pairs remain pairs and stay in the ground state, unable to scatter.

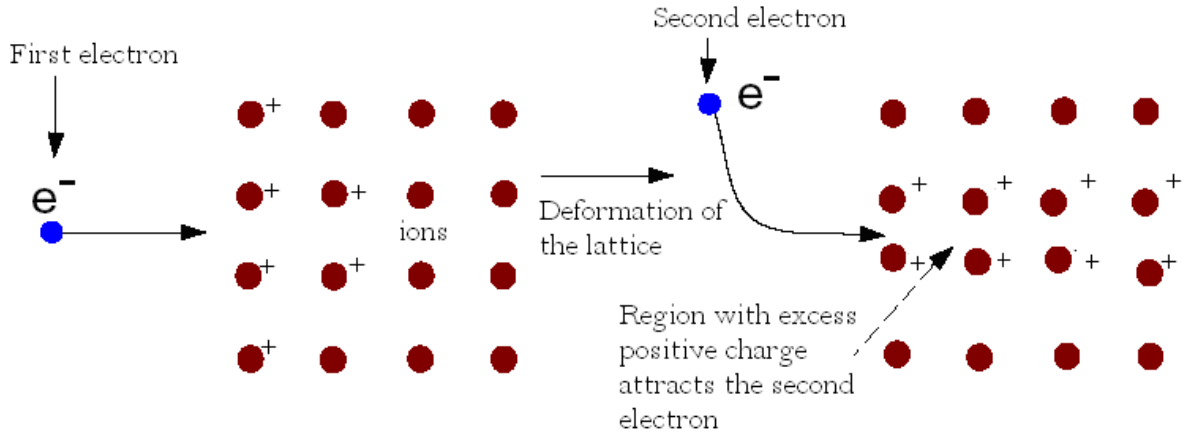

Figure 10: Formation of a Cooper Pair. Adapted from [16].

The mechanism that binds the electrons into such pairs, named Cooper pairs, was first proposed by Herbert Fröhlich, and is illustrated in figure 10. He suggested that the two electrons might be coupled by a phonon, a lattice vibration quantum. This proceeds as follows: an electron passes through the lattice of positively charged ions, deforming it as it goes. The deformed lattice has a surplus of charge where the ions have been pulled closer together, and this attracts another electron. The two electrons and the vibration or phonon moving with them together form the Cooper pair. The binding energy for such an interaction is very small, on the order of 0.01 eV, and the distance between electrons can be many times the lattice parameter.
In BCS theory, proposed by Bardeen, Cooper and Schieffer, the macroscopic wavefunction of the entire sea of electrons is considered, while assuming the existence of Cooper pairs and their immediate condensation when they are formed below T_c. What results is a gap in the Density of States (DOS) at the Fermi energy.

3.2 STM and STS

Figure 11a schematically shows how the potential varies between two conductors, with an insulating layer of, for instance, air or vacuum in between. The high barrier caused by the insulator prevents electrons from crossing from one conductor to the next. However, an electron, seen as a wave, decays exponentially into the barrier, and when it decays sufficiently little because the barrier is very thin, on the order of a few nanometers as in figure 11b, it may appear again on the other side of the barrier.

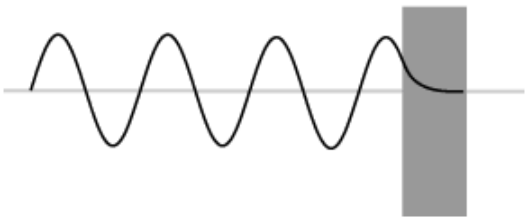

Figure 11a: Electron decays in a potential barrier.

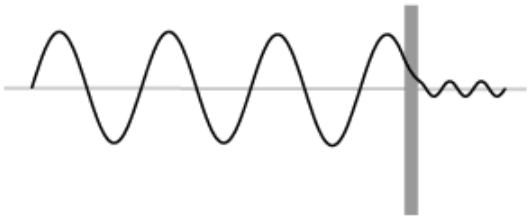

Figure 11b: Electron passes a very thin potential barrier [17].

When performing Scanning Tunneling Microscopy (STM), the conducting media are the tip and sample as depicted in figure 12, brought into such very close contact so that an electron can easily tunnel through the vacuum in between. This gives rise to a current signal, which is proportional to the convolution of the DOS of the tip and that of the sample at the point of measurement. 90% of the current is generated by electrons tunnelling between the last atom of the tip and the surface, and for this reason the DOS of the tip can be approximated by a delta function. A convolution of such a function with any DOS of the sample will result in a current signal only dependent on the sample. There are two ways this can provide you with an image of the DOS of the area scanned by the tip: either one keeps the distance to the sample fixed and records the variations in current, or the current between tip and sample is kept constant by constantly changing the height of the tip and the tip height is imaged. Using STM, we search for flat regions of MgB_2 where we can be sure to have a well ordered $MgB_2(0001)$ surface.

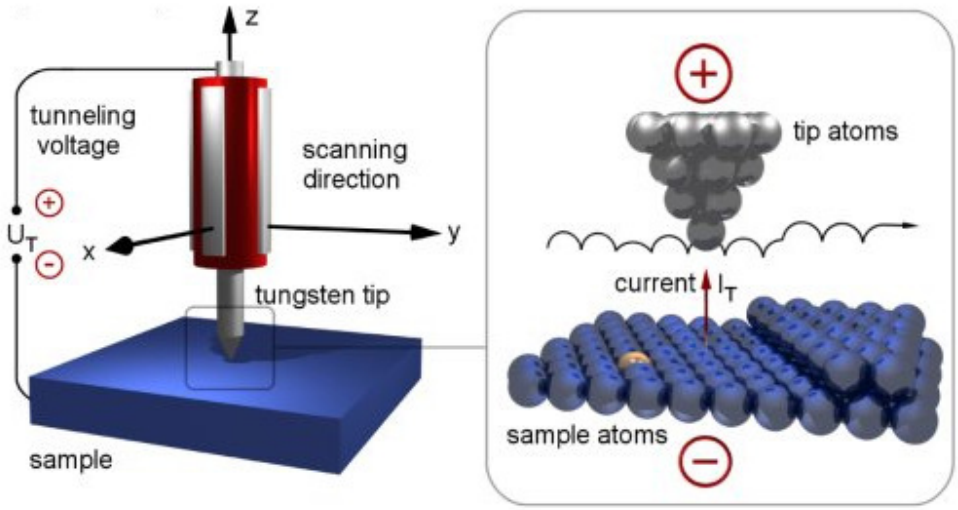

Figure 12: The scanning tunneling microscope [18].

To directly see the superconductive gap, we can see from the following formulas (describing tunneling from a metal, through a barrier, to a superconductor [19]) that the derivative of current versus bias voltage is proportional to the DOS:

$$dI/dV \sim C\,\rho(E)$$

$$\rho(E) = \begin{cases} E/(E^2 - \Delta^2)^{1/2} & (E > \Delta) \\ 0 & (E < \Delta) \end{cases}$$

Here C is conductivity, $\rho(E)$ is the DOS, Δ is a parameter describing the width of the gap, and E is the energy relative to the Fermi level, directly related to the applied bias voltage. The relation between current and voltage these formulas predict is shown schematically in figure 13a and 13b

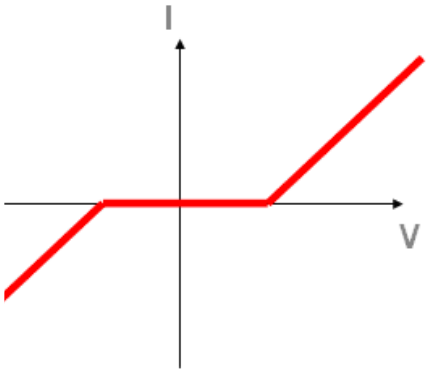

Figure 13a: The general behaviour of current versus voltage when tunneling from a conductor to a superconductor. There is a clear kink in the plot at zero bias voltage.

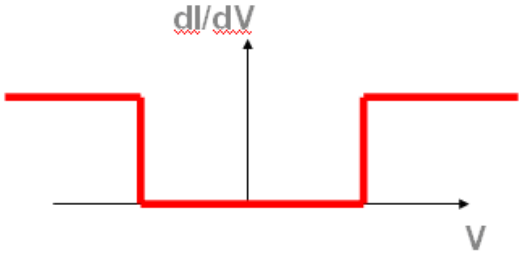

Figure 13b: The derivative of figure 13a, showing the superconductive gap [12].

.

To obtain such a dI/dV versus voltage plot, we use the microscope to perform Scanning Tunneling Spectroscopy (STS). The STS measurements consist of keeping the tip fixed at the chosen location, varying the voltage between tip and sample, and measuring the resulting current. Part of the output of a Lock-In Detector is the derivative dI/dV [20], so we used one to try and directly see the superconductive gap. Since magnesium has no known critical temperature for superconduction, seeing a superconductive gap is also another confirmation that one is indeed measuring on a good MgB_2 sample.

The actual identification of the material is done by analyzing height differences seen with STM. When a step in the (0001)-direction, seen by STM, corresponds very closely with the thickness of a single sheet of either magnesium or MgB_2, we can identify that region as such. We calculated the thicknesses of the sheets of magnesium and MgB_2 as half the lattice parameters seen in figures 2a and 2b: 2.59Å for a single sheet of magnesium and 1.76Å for a single sheet of MgB_2, which is compatible with surface XRD measurements done in MgB_2 thin films [21].

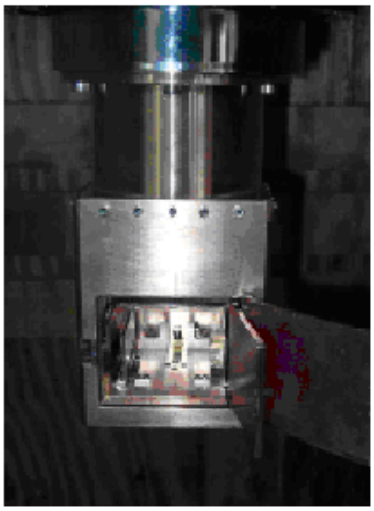

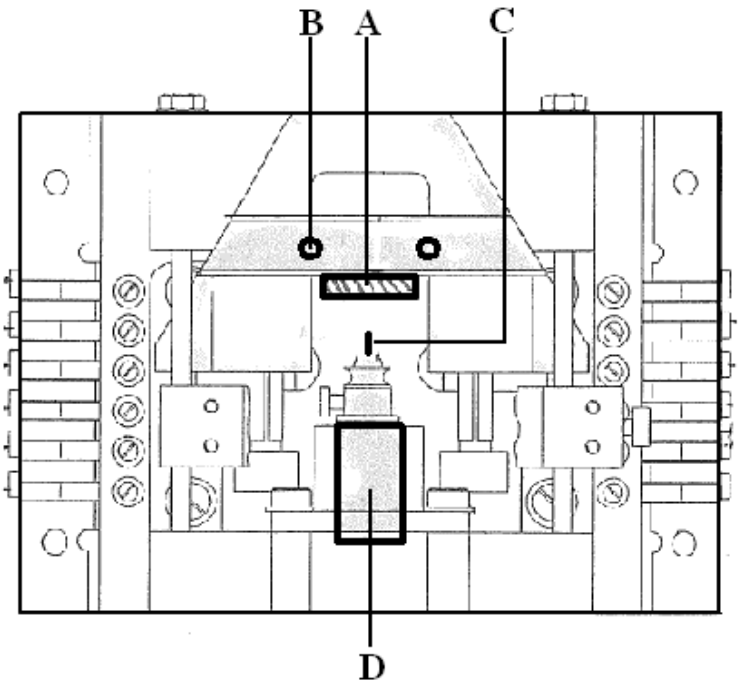

Figure 14a: The microscope chamber. **Figure 14b: The microscope chamber schematically.**

Figure 14a shows the small chamber housing the microscope we used. The sample, denoted by A in figure 14b, is lowered onto a pronged platform (B), after which it can be slowly approached by the tip (C) using piezomotors (D). This type of motor is capable of minute movement and moves the tip to within nanometers from the sample automatically, since such movement is too fine to be seen by eye and controlled by hand. The tip is tungsten, and has been chemically sharpened. This tip is then scanned along the sample by additional piezomotors.

To achieve the low temperatures necessary for superconductivity, the microscope chamber in figure 8a is part of a larger cryostat. The cryostat is made up of two compartments, one inside the other. The outer compartment is filled with liquid nitrogen, which has a temperature of 77 K. The function of the nitrogen is to isolate the inner compartment from room temperature, since the latter is filled with liquid helium, which is at 4.2 K. The inside temperatures are measured using thermocouples, and if the liquids are seen to be boiling, and thereby disrupting measurements, they can be pumped to lower their temperatures again using a turbo pump.

Results

4.1 Quality of the MgB_2 thin films as judged by AES and LEED

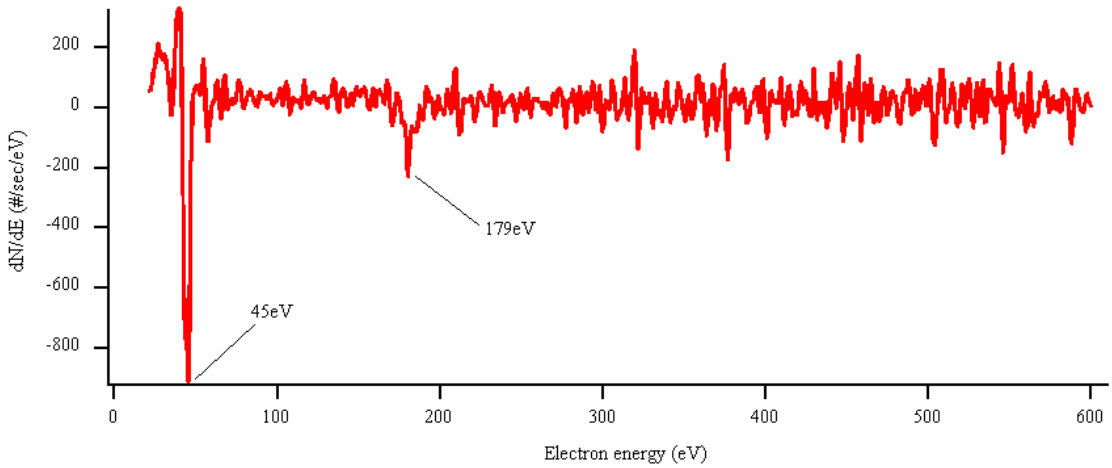

Figure 15: dN/dE derived from green AES spectrum in figure 16.

Before we go to the trouble of inserting the finished sample into the microscope, it is necessary to check its quality by means of Auger and LEED. Figure 15 shows the plot of dN/dE versus electron energy, derived from an Auger spectrum taken after two hours of co-deposition of magnesium and boron on Mg(0001). Clearly visible despite the noise are the peak for magnesium at 45 eV and the peak for boron at 179 eV.
Also clear from this graph is that there are no sizable amounts of contaminants on our sample. The presence of oxygen would cause several peaks at 500 eV, as would argon remaining from the sputtering of the substrate at 215 eV [11]. The lack of any extra peaks indicates the sample is clean.

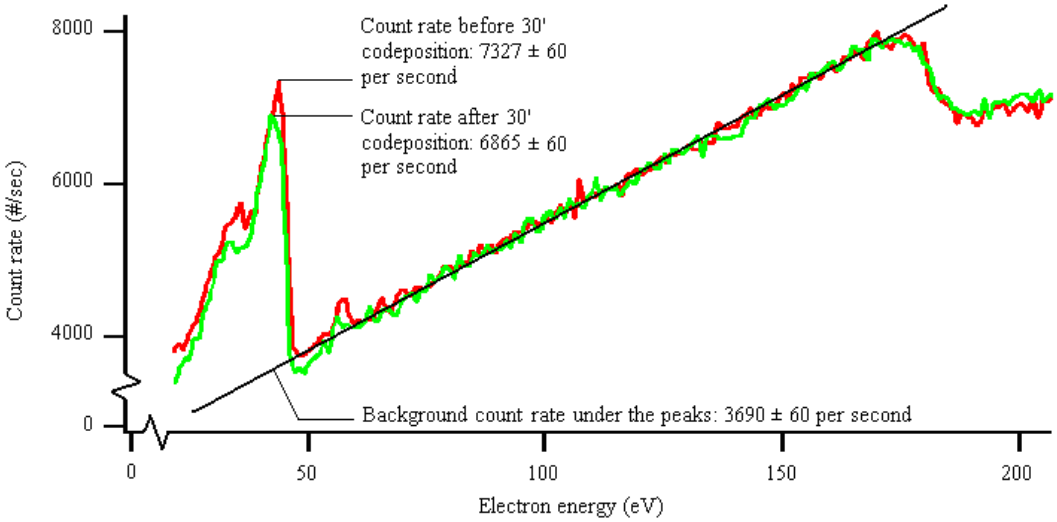

Figure 16: AES spectra after 1h (red) and after then another 30 minutes (green) of co-deposition of Mg and B on Mg(0001).

Figure 16 shows two Auger spectra of count rate versus electron energy from the same measurement shown in figure 15. The red spectrum was taken after 1h, the green spectrum after 1h 30' of co-deposition. The peak corresponding to magnesium is clearly lower afterwards, indicating the substrate has been further covered by boron. A formula to estimate this is the following [22]:

$$I = I_0 \, e^{-d/\lambda}$$

Here I is the signal intensity, I_0 is the singnal intensity before deposition, d is the thickness of the layer of deposited boron, and λ is the electron mean free path, in this case 5.3Å [23]. Inserting the values given in figure 16, we calculate the growth in this half hour of co-deposition to be 0.41 ± 0.08 ML of boron, meaning we have a growth speed of 0.82 ± 0.16 ML / h.

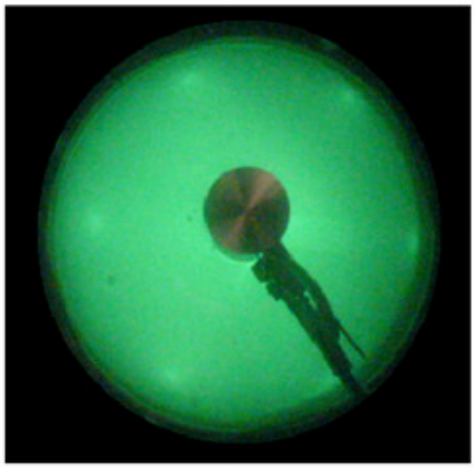

Figure 17: LEED pattern of an MgB_2(0001) epitaxial thin film grown on Mg(0001) after two hours of co-deposition of Mg and B.

Figure 17 shows the LEED pattern which is, as the Auger spectra in figure 13, common to every sample we then performed STM and STS on. As said before, in the case of MgB_2 and magnesium, we expect a hexagonal pattern to form. This is exactly what we see, well discernible from the background, so the lattice in general has the correct shape. To estimate the size of the domains, we would need to perform an analysis of the pattern intensity, which is not possible with the image shown here, but is a good idea for future research into these samples. With our simple approach to LEED, we cannot draw any further quantitative or more precise conclusions about the lattice, so after this initial checking we turned to STM to see if we could directly identify MgB_2.

4.2 Analysis by STM

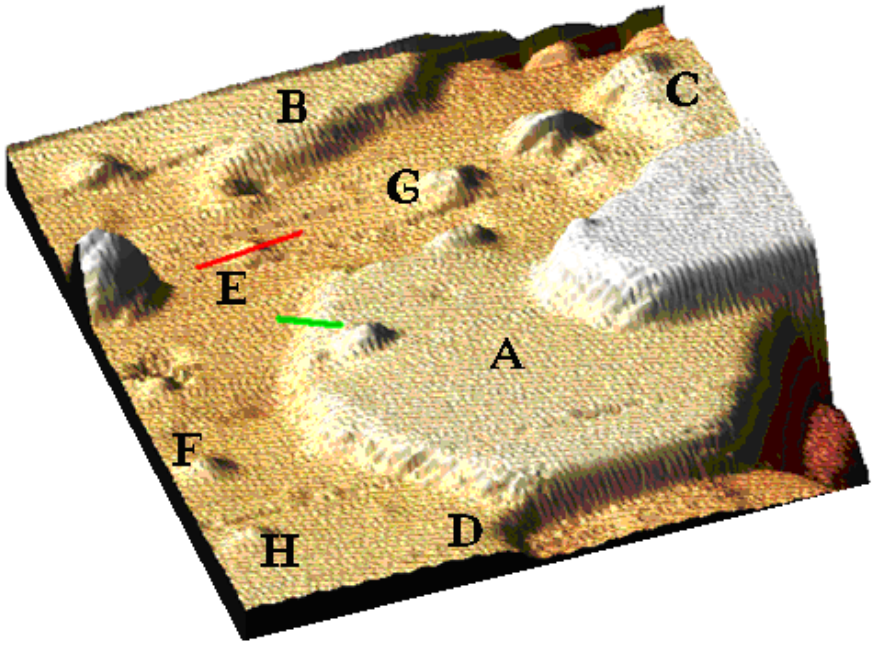

Figure 18: 3D room temperature STM image (25 x 25 nm) of a MgB_2(0001) epitaxial thin film grown on Mg(0001) by 4h of co-deposition of Mg and B. Bias voltage when scanning was 800 mV, set current 70 pA. The large hexagonal island is clear magnesium. Thanks to [24] for the software.

Figure 18 represents a room temperature STM image of a MgB_2(0001) epitaxial thin film grown on Mg(0001) by 4 hours of co-deposition of magnesium and boron. The expected hexagonal symmetry is immediately obvious in the large island, labeled A, in the bottom right corner. To see if we are dealing with magnesium or MgB_2, we look at the height of the island, along the indicated green line.
In figure 19a the profile of the height along the green line in figure 18 is shown. Here, the step height matches the characteristic height for a single sheet of magnesium of 2.59Å, and we could verify by checking further height profiles from figure 18 that the height is the same along the edge of the island, indicating that it is an island of magnesium. As is also clearly visible in figure 18, many of the other discernible height differences in the image, namely those at locations labeled B, C and D, correspond to this magnesium step height. Of one of the few smaller protrusions labeled E, F, G and H that show in figure 18, figure 19b gives a representative height profile, along the red line in figure 18. The step height is much smaller than either magnesium or MgB_2, and we assume it to be a contaminant.
A possible explanation for this kind of magnesium island to form on top of the sample is that we kept the magnesium evaporator on longer than the boron evaporator. At the temperature needed to grow MgB_2 magnesium may sublimate, so this way we can be more sure of the stoichiometry of the film. This extra deposited magnesium may be what we see in figure 18. However, no steps here match the MgB_2 step height of 1.76Å.

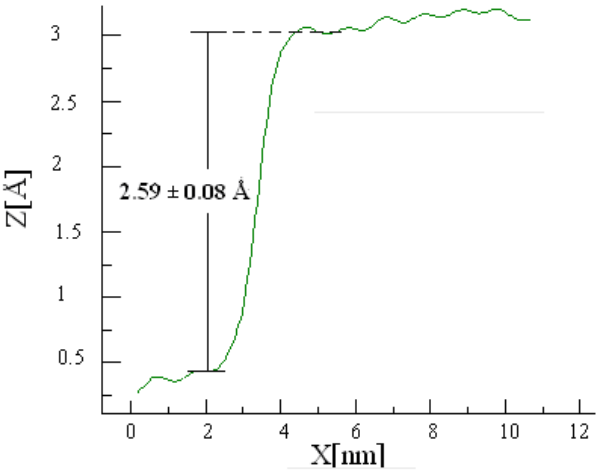

Figure 19a: Height profile for green line in figure 18. The step height corresponds very closely to the height of a sheet of Mg, so we can identify the island as magnesium. [25].

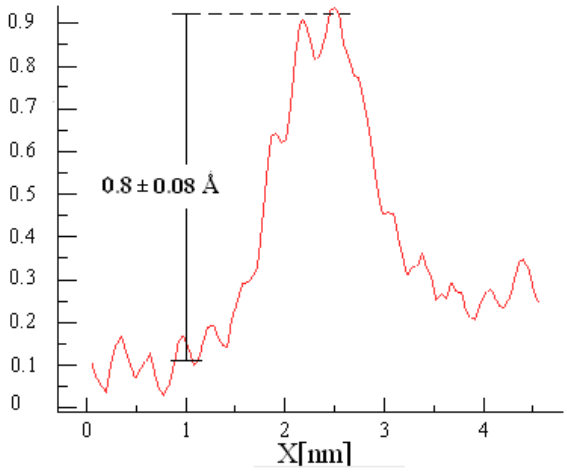

Figure 19b: Height profile for red line in figure 18 Such a small island, too low to be a Mg or B, must be a contamination.

A more interesting set of islands showing hexagonal symmetry can be seen in the STM image shown in figure 20, which refers to a MgB_2 film produced by co-depositing for 2 hours. The two hexagonal islands are labeled in their centres as A end B. Figure 21a shows the height profile along the red line in figure 20 at the edge labeled C, where we again recognize the lattice parameter for magnesium. Figure 21b shows the height profile along the blue line at the edge labeled D, and here we see the MgB_2 lattice parameter, indicating succesful growth of MgB_2. However, both materials seem to be mixed, and the ridges criss-crossing the islands at the locations labeled E, F anf G in figure 20 indicate how.

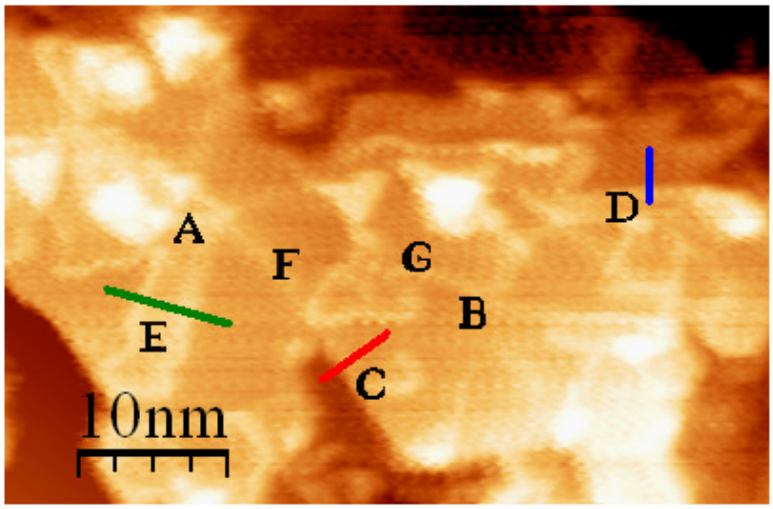

Figure 20: Room temperature STM image collected from a (0001) epitaxial thin film grown on Mg(0001) by 2h of co-deposition of Mg and B. Bias voltage when scanning was 800 mV, set current 80 pA. Dislocations are clearly visible on the hexagonal islands.

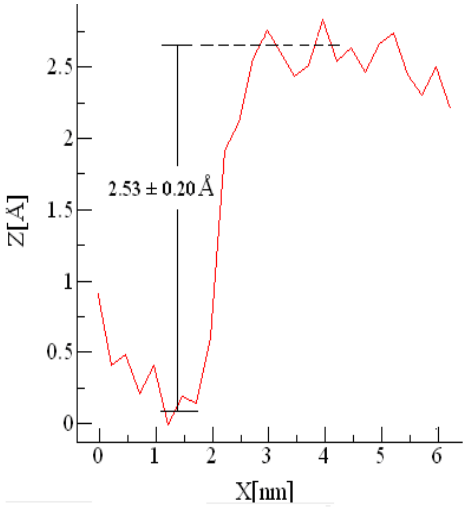

Figure 21a: Height profile along the red line in figure 20. The height of the island matches the magnesium step height.

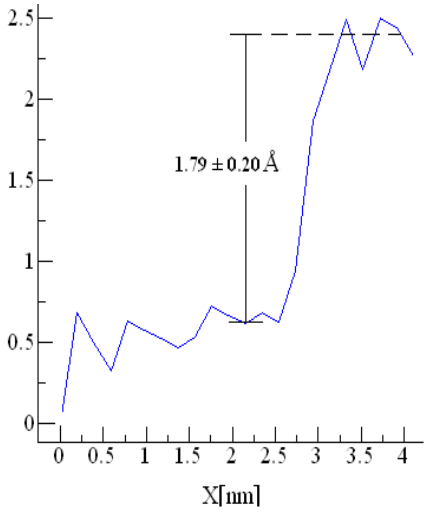

Figure 21b: Height profile along the blue line in figure 20. The height of the island matches the step height of MgB_2.

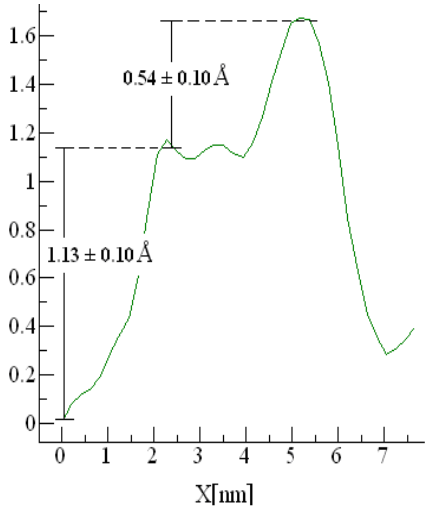

Figure 21c: Height profile along the green line in figure 20 along a ridge. The height differences are too small to come from stacked sheets of magnesium or MgB_2, and must follow from dislocations.

Figure 21c shows the height profile along one of these ridges, along the green line in figure 20. As with the protrusions in figure 18, we see from figure 21c that the step height of these ridges is too small to be either magnesium or MgB_2. However, whereas a protrusion can be written off as a contaminant, such a ridge of many nanometers long along the crystal can be a fault line between materials with a different lattice parameter in the (0001)-direction, as illustrated in figure 22. We can conclude that the two materials are grown simultaneously, and that wether the crystal orders itself into MgB_2 or Mg can vary every couple of unit cells. Since we need large flat planes to measure a bulk effect on, this is not yet a satisfactory result.

Figure 22: Illustration of ridge-forming along the surface [26].

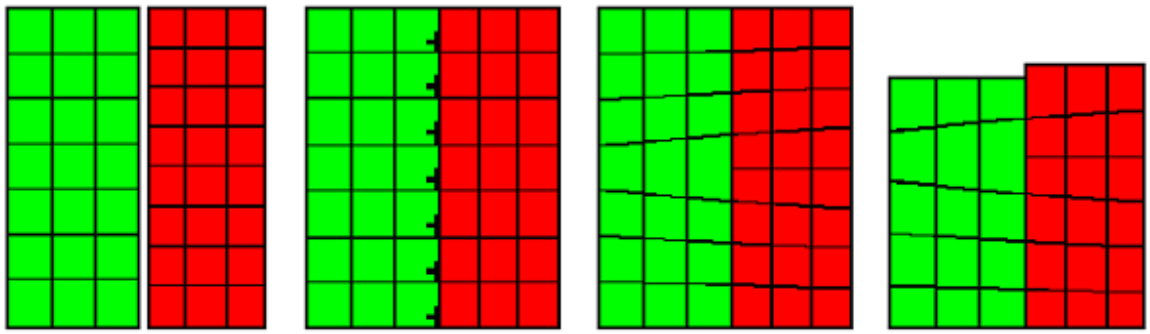

Two materials with a different lattice parameter.

When grown together, these small dislocations are necessary to make the lattices fit against each other.

The stress of these dislocations is relieved by dislocation misfits (in the middle of the figure).

At the surface,, this may cause one material to protrude along the edge.

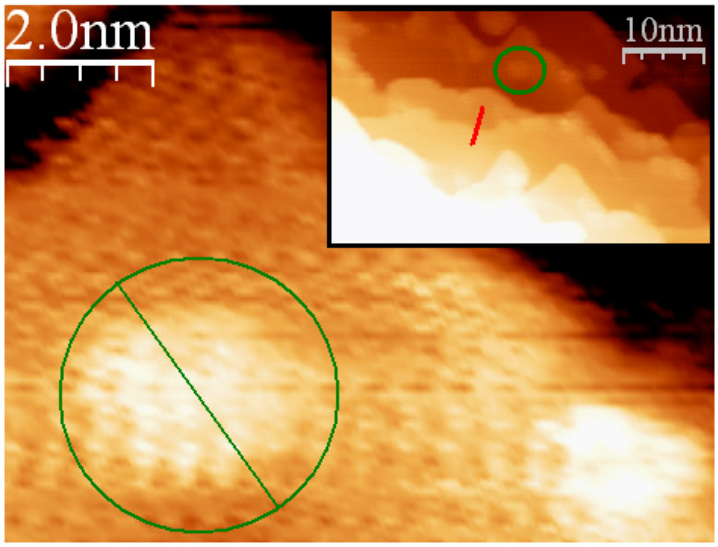

Figure 23: Room temperature STM image collected from a (0001) epitaxial thin film grown on Mg(0001) by 2h of deposition of B. Bias voltage when scanning was 1000 mV, set current 100 pA. We see a small MgB_2 island along the green straight line (the green circle is enlarged from the inset in the upper right corner), and a ridge of MgB_2 along the red line in the inset.

Since the result most indicative of successfully growing layers of MgB_2 by co-depositing was the one just shown in figure 20, we also tried to do a simple deposition of only boron onto the magnesium substrate, to see if we could produce a more homogeneous film of MgB_2. Figure 23 shows the result of this simpler deposition, which had gone on for half an hour; with the image taken at room temperature. It shows two important features: firstly, there is the height profile of the island enlarged from the inset in the upper right corner, along the green straight line, given by figure 24a; secondly, figure 24b shows the height profile of the ridge of some 20 nm long in the inset itself, along the red line. In both we see steps which very nearly match the characteristic step height of MgB_2, 1.76Å, indicating growth of layers of MgB_2.

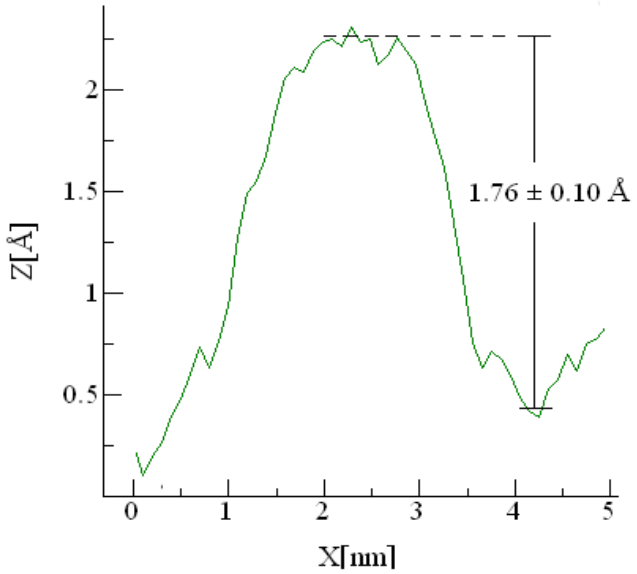

Figure 24a: Height profile for figure 23 along the green line. The height of the island matches the MgB_2 step height.

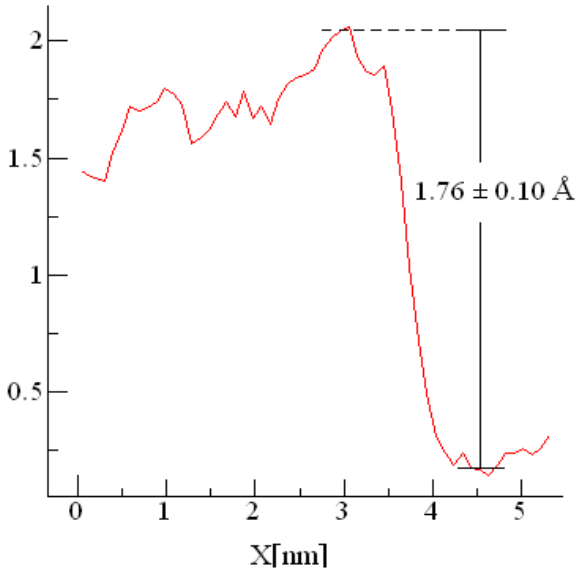

Figure 24b: Height profile for figure 23 along the red line. The ridge matches the MgB_2 step height.

4.3 Analysis by STS

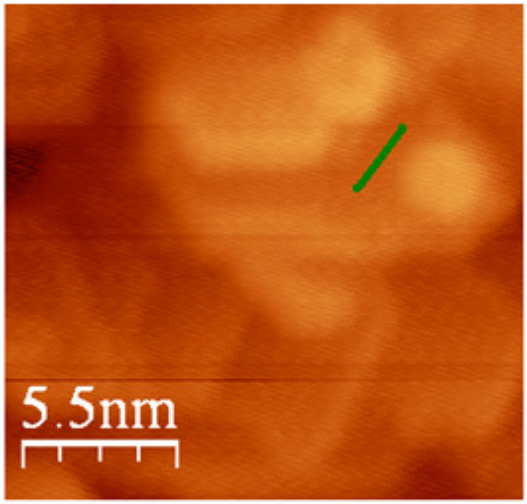

Figure 25: STM image taken at 4.2 K collected from a (0001) epitaxial thin film grown on Mg(0001) by 4h of co-deposition of of Mg and B. Bias voltage when scanning was 20 V, set current 17 pA. You can see much noise on the surface, lines from the upper left to the lower right.

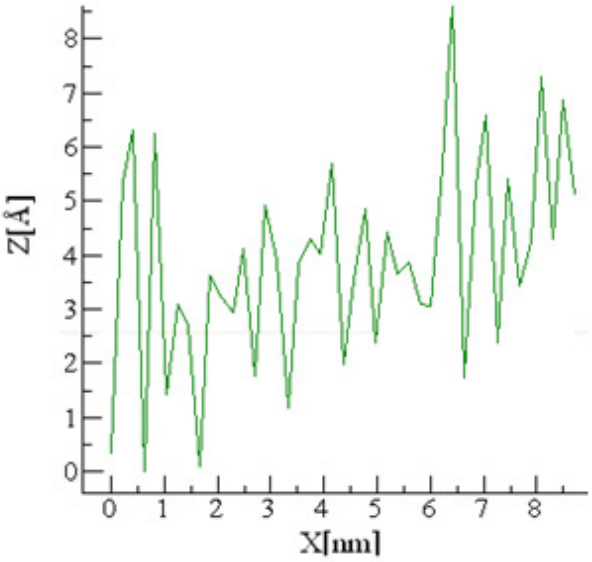

Figure 26: Height profile for figure 25 along the green line. The noise is many times the step height for MgB2.

We made several attempts to perform STS on samples where we could be reasonably sure there was MgB_2 on the surface. However, none of these were successful. Indicative measurements were performed on the sample in figure 25, where we had co-deposited Mg and B for four hours, and the AES and LEED were similar to the ones shown in figures 16 and 17, respectively. Figure 26 shows the height profile along the green line in figure 25, a line that does not cross any ridges, and should therefore not have significant height differences along it. However, the noise in figure 26 is several times larger that the steps in height we try to find, so certain identification of MgB_2 using STM is not possible, and looking for a superconductive gap becomes impossible.

Figure 27 shows what the dI/dV-curve obtained by STS and the Lock-In should look like, with the dots signifying actual measurements and the line drawn through them a fit by a BCS quasiparticle density of states. From this we know that the gap should be located within 5 mV from the origin, and curve down nearly to 0, with two clear shoulders at the sides. Since the gap is a derivative of current over voltage and is symmetric around the y-axis, we expect the original function of voltage versus current to be a straight line that has a kink over the origin.

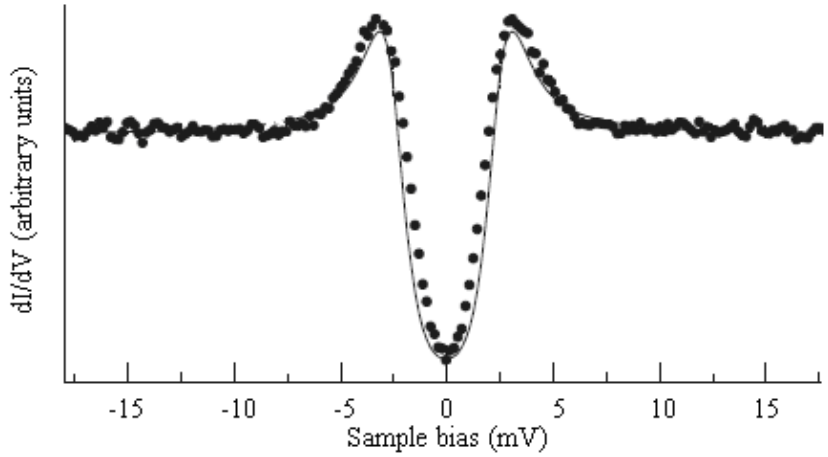

Figure 27: The known gap for MgB_2 at 4.2K, adapted from [27].

In figure 28a we see our result of STS performed on the sample in figure 25, with the green and red lines representing two separate scans, green from negative to positive, and red from positive to negative. There is no clearly visible kink over the origin, and as the bias voltage increases, so does the noise, as can be seen near the edges of the plot. The slight ribbon shape made by the forward and backward scans indicates the sample is still moving because of the cooling down of the sample, after waiting for around four hours.
Figure 28b shows the derivative of this IV-curve, obtained directly by a Lock-In detector. There is no visible dip in the signal over the origin and the shoulders are invisible as well. There also seems to be added noise coming from the Lock-In itself, since the noise in the middle of figure 28b seems no less than that at the edges, while we would expect it to be less, judging from the lack of noise in the middle of figure 28a. In any event, from our measurements it is not possible to see the superconductive gap.

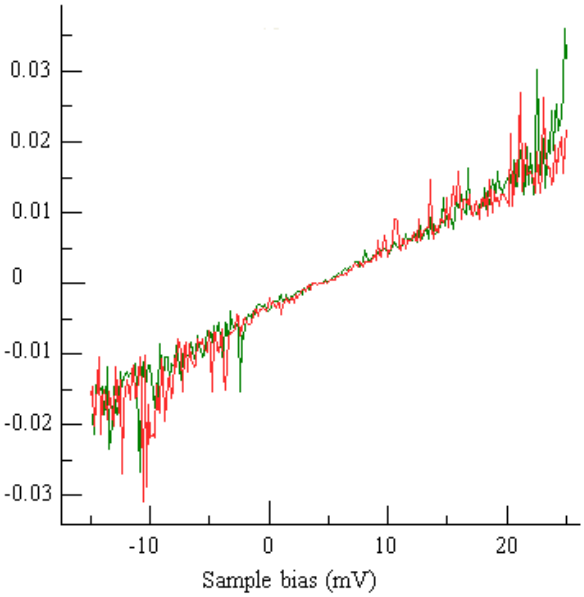

Figure 28a: I-V curve taken on the sample shown in figure 25. There is no kink at the origin and at the edges there is much noise.

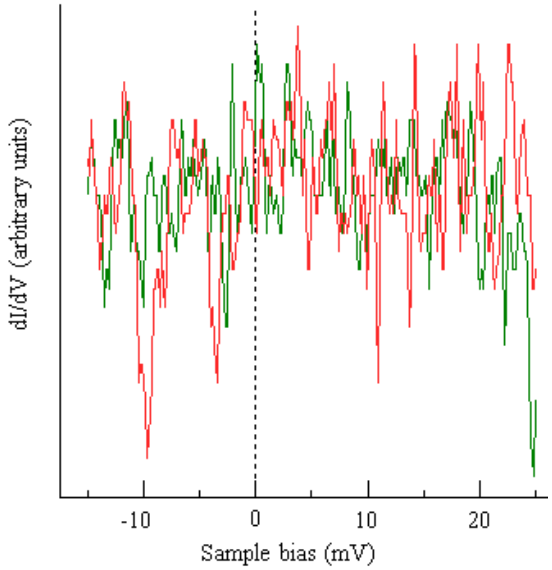

Figure 28b: derivative of 28a, taken by Lock-In Detector.

Conclusions

The first challenge of this project was to successfully co-deposit magnesium and boron to form epitaxial thin films of MgB_2 on Mg(0001), a novel approach for this material. From our results presented in the last sections, even though AES and LEED gave strong indications for a MgB_2 film in terms of surface composition and symmetry of the lattice, we could not manage to identify sheets of MgB_2 in our STM images by looking at height differences. Indications for the presence of MgB_2 can be found in the form of fault lines, though. Depositing only boron gave better results, since we could actually see islands and sheets of MgB_2, yet this technique is only useful for making very thin layers of very few monolayers. Since our aim was to find the relation between superconductivity and sample thickness, this is not a very important success.
Several factors need to be improved upon before growing MgB_2 by co-deposition in this way becomes viable. First of all, we did not have an exact method to determine the temperature of the sample during the co-deposition, while it is a very crucial parameter due to the small window of pressure and temperature where MgB_2 forms. In this respect our research has largely been based on trial and error, and with more control over the sample temperature, a rigorous protocol can be developed. Furthermore, we had continuing problems with our boron evaporator, which sometimes gave us results such as discussed above, but which sometimes after depositing for several hours seemed to have deposited almost nothing on the substrate, judging from the Auger spectrum. The fact that the amount of deposited boron varied very much per co-deposition, with all parameters kept constant, lead to doubts about the quality of the evaporator. The rod of boron and the filament might not have been aligned well enough, causing some portions of the boron in the evaporator to be heated too much by the filament and melt, since several times a piece of boron fell from the evaporator into the chamber. A new, well aligned, well calibrated source for boron might quickly lead to better results. Furthermore, since our research tries to make statements about a dependence on thickness of the sample, this calibration is especially important, and has so far not been reliable.
The determination of a superconductive gap which we wanted to relate to the sample thickness has so far eluded us. Perhaps the MgB_2 was not yet grown well enough to allow for superconductivity, or if it was, it was so local that we could not find it. Aside from the quality of the sample, most dI/dV-curves were rendered unusable because of drift in the samples after cooling down, both by shrinking of the sample itself and because of the piëzomotors, or because of noise, the origin of which (mechanical, electronic or both) we were not able to determine. We propose some techniques for removing noise might be successfully implemented to yield good measurements.
To lessen mechanical noise, further decoupling the chambers from the room around them might prove a good idea, since many cables run from chambers to room of necessity, which can pass vibrations from the building to the microscope chamber if not damped well enough. Electronic noise might be further eliminated by adding passband filters, or other circuits that dampen or eliminate certain frequencies, to the Lock-In detector used to take the derivative, since it seems picking up additional noise, as can be seen from figures 22a and 22b.
While this research itself will of course be continued, future research on MgB_2 and its unique superconductive properties has already been planned. At the end of this year, at the Elettra BEAR synchrotron beamline, the electronic structure of MgB_2 epitaxial films will be researched in more detail by means of Near-Edge X-ray Absorption Spectroscopy, while at the BADELPH beamline the superconductive gap will be investigated using Angle Resolved Photon Emission Spectroscopy. The results of this research should give more insight into the characteristics of thin films of MgB_2, grown epitaxially on Mg(0001).

References and word of thanks

[1] J. Nagamatsu *et al.,* Nature (London) 410, 63 (2001).
[2] J. G. Bednorz and K. A. Mueller, Z. Phys. B: Condens. Matter 64, 189 (1986).
[3] H. K Amimura, H. U Shio, S. M Atsuno, and T. H Amada, *Theory of Copper Oxide Superconductors*, Springer-Verlag, Berlin (2005).
[4] K. Szałowski, *Critical temperature of MgB_2 ultrathin superconducting films: BCS model calculations in the tight-binding approximation*, physical review B 74, 094501 _2006_
[5] C. Buzea and T. Yamashita, *Review of superconducting properties of MgB_2, Submitted to Superconductor, Science & Technology,* Received 15 August 2001
[6] F. Giubileo, D. Roditchev, W. Sacks, R. Lamy, J. Klein*, Strong coupling and double-gap density of states in superconducting MgB2*, Europhys. Lett., 58 (5), pp. 764–770 (2002).
[7] M. Naito and K. Ueda, *Growth and Properties of Superconducting MgB2 Thin Films,* NTT Basic Research Laboratories, NTT Corporation, 3-1 Wakamiya, Morinosato, Atsugi, Kanagawa 243-0198, Japan.
[8] http://www.tasc.infm.it/info/doc/Report2007-preprint.pdf.
[9] K. Ueda and M. Naito, J. Appl. Phys. 93, 2113 (2003).
[10] http://en.wikipedia.org/wiki/Image:Auger_Process.svg.
[11] L.E. Davis, N.C. MacDonald, P.W. Palmberg, G.E. Riach, and R.E. Weber, *Handbook of Auger Electron Spectroscopy* (Physical Electronics Industries, Inc., Minnesota, 1976), 2nd ed.
[12] Viewgraph of "Surfaces and Interfaces" course, P.Rudolf, RUG 2007.
[13] http://www.phytem.ens-cachan.fr/telechargement/Module_PhysNum/LEED.pdf.
[14] J.-K. Zuo and J.F. Wendelken, Phys. Rev. 66, 17 (1991).
[15] J. Bardeen, L.N. Cooper, J.R. Schrieffer, Phys. Rev. 108, 1175 (1957)
[16] R. Macovez, *Film Sottili Del Composto Superconduttivo* MgB_2*: Crescita Epitassiale e Caratterizzazione Mediante Technice di Spettroscopia Elettronica,*Thesi in Lauria di Physica, anno accademico 2002-2003.
[17] http://www.nanoscience.com/education/i/wavefunc.gif.
[18] www.ieap.uni-kiel.de/surface/ag-kipp/stm/stm.htm
[19] Lecture notes of "Superconductivity" course, D. van der Marel, Université de Genève 2001.
[20] Lecture notes of "Principles of Measurement Systems" course, E. Kerstel, RUG 2007.
[21] L.Petaccia, C. Cepek, S. Lizzit, R. Larciprete, R. Macovez, M. Sancrotti, A. Goldoni, New Journal of Physics 8 (2006) 12.
[22] K. Oura, V.G. Lifshits, A.A. Saranin, A.V. Zotov, M. Katayama, *Surface Science an Introduction*, Springer-Verlag Berlin Heidelberg (2003).
[23] Tanuma, Powell and Penn, Surface Interface Analysis, 21 (1994) 165.
[24] I. Horcas et al., Rev. Sci. Instrum. 78, 013705 (2007)
[25] The height profiles shown have had noise removed from them by averaging the height over an range of 2 nanometers wide along the profile.
[26] D. Hull and D. J. Bacon, *Introduction to dislocations, 4th edition*, Elsevier Ltd., London (2001).
[27] F. Bobba, D. Roditchev, R. Lamy, E.-M. Choi, H.-J. Kim, W.N. Kang, V. Ferrando, C. Ferdeghini, F. Giubileo, W. Sacks, S.-I. Lee, J. Klein and A.M. Cucolo*, Quasiparticle state density on the surface of superconducting thin films of MgB_2*, Supercond. Sci. Technol. 16 (2003) 167–170

I would like to express my heartfelt thanks to Prof. Dr. Petra Rudolf, for giving me the possibility to work abroad, it was a remarkable experience. Also my thanks go to Dr. Cinzia Cepek for guiding and helping me at TASC, and to Mattia Fanetti, with whom it was a pleasure to endure the long searches for superconductivity, and to Prof. Silvio Modesti for watching over us during our efforts.

And at the very end, I would like to thank my father, Gerrit Jan Zwier, without whose help and support this thesis would be exactly the same.